Mansoura University

Mansoura Journal Of Chemistry

Synthesis, Spectral characterization, Computational calculations and Biological Activity of Complexes Designed from Nno Donor Schiff-Base Ligand

Ola A. El-Gammal*, G.M.Abu El-Reach , T.A.Youssef and M.M.Sarhan
Department of Chemistry, Faculty of Science, Mansoura University, Mansoura, 35566, P.O.Box 70, Mansoura- Egypt.

Received 10 August 2014; accepted 17 August 2014

keywords
Hydrazone derivatives; Coats-Redfern; Horowitz-Metzger; DFT molecular modeling; antioxidant and antitumor activity.

Abstract A new series of Co(II), Ni(II) and Cu(II) complexes of (Z)-2-oxo-2-(phenylamino)-N'-(1-(pyridin-2-yl) ethylidene)acetohydrazide(H_2OPPAH) have been prepared and characterized by conventional techniques.The spectral data indicated that the ligand acts as neutral or mononegative NNO tridentate. On the basis of magnetic and electronic spectral data an octahedral geometry for Ni(II) and Cu(II) complexes and a tetrahedral geometry for Co(II) complex have been proposed. The molecular modeling using DFT calculations were carried out for the Schiff base ligand and its metal complexes. The Kinetic and thermodynamic parameters were determined for each thermal degradation stages of the ligand and its complexes using Coats-Redfern and Horowitz-Metzger methods. Also, the compounds were screened for antioxidant activity using ABTS free radical, anti-hemolytic, and *in vitro* cytotoxic assay. H_2OPPAH showed the potent antioxidant activity followed by Co(II) and Cu(II) complexes. On the other hand Ni(II) complex exhibited weak antioxidant activity using ABTS free radical and erlich and strong erythrocyte hemolysis activity.

*****To whom correspondence should be addressed:
E-mail: olaelgammal@yahoo.com

1. Introduction

Compounds containing hydrazone moiety find wide applications in the treatment of diseases such as tuberculosis as they are herbicides, insecticides, plant growth regulators and possess antifungal and antibacterial activities(Vicini et al., 2006 and Bezerra-Netto et al., 2006) Also, their derivatives have been applied successfully in the analytical chemistry as reagents for selective chemical separations (Pinto et al., 2004) Moreover, they used for the spectrophotometric micro determination of some metal ions (Basu et al., 2007 ; Pouralimardan et al., 2007 and Terra et al., 2002) and in polymer industry (Getautis et al., 2008).Certain hydrazones and their copper (II) complexes have antitumor activity (Buss et al., 2002).The biological activities, chemical and industrial applications of metal hydrazone complexes for example, Schiff base hydrazones of pyridoxal phosphate and its analogous have been studied to better understand the mechanism of action for vitamin B_6-containing free ligand. Also, metal complexes of hydrazones proved to have potential

applications as catalysts (Whitnall et al., 2006), luminescent probes (Spek 1998), and molecular sensors (Pérez-Rebolledo et al., 2006). In addition, it has been recently shown that hydrazones iron chelators *in vivo* and *in vitro*, and may be of value for the treatment of iron overload (El-Gammal 2010). Furthermore, some 2-formylpyridine derived hydrazones which behave as iron chelators were suggested as therapeutic agents for the treatment of neurodegenerative disorders .On continuation to our work on 2-acetylpyridine hydrazone derivatives (El-Gammal et al., 2012), we report herein the chelating properties of (Z)-2-oxo-2-(phenylamino)-N'-(1-(pyridin-2-yl)ethylidene)acetohydrazide (H_2OPPAH) towards Co(II), Cu(II) and Ni(II) metal ions in more details, including structural elucidation, thermal behavior and molecular modeling. Also, the antioxidant activity evaluated using ABTS (2- azino-bis (3-ethylbenzthiazoline)-6-sulfonic acid) and anti-hemolytic as well as cytotoxic activities of the compounds have been discussed.

2. Experimental

2.1. Materials and methods

All the chemicals were purchased from Aldrich and Fluka and used without further purification. Elemental analyses (C and H) were performed with a Perkin-Elmer 2400 series II analyzer. IR spectra (4000 - 400 cm^{-1}) for KBr discs were recorded on a Mattson 5000 FTIR spectrophotometer. Electronic spectra were recorded on a Unicam UV-Vis spectrophotometer UV2.Magnetic susceptibilities were measured with a Sherwood scientific magnetic susceptibility balance at 298 K. ^{1}H NMR measurements in d_6-DMSO at room temperature were carried out on a Varian Gemini WM-200 MHz spectrometer at the Microanalytical Unit, Cairo University. Thermogravimetric measurements (TGA, DTA, 20-1000^{o}C) were recorded on a DTG-50 Shimadzu thermogravimetric analyzer at a heating rate of 10^{o}C/min and nitrogen flow rate of 20 ml/min.

2.2. Synthesis of H_2OPPAH

2-hydrazino-2-oxo-N-phenyl-acetamide was synthesized according to the general literature method **(Cescon & Day, 1962)**. H_2OPPAH was synthesized by heating under reflux for 8h an ethanolic solution of 2-hydrazino-2-oxo-N-phenyl-acetamide (1.79gram, 1mmol) and 2-acetylpyridine (0.13 ml, 1.21 mmol) in 1:1 molar ratio with adding few drops of glacial acetic acid. Upon cooling, a white solid was precipitated. The product formed was filtered off, washed several times with ethanol, recrystallized from hot ethanol and finally dried in vacuum desiccator over anhydrous $CaCl_2$.The purity was checked by TLC. The melting point is 260 ºC.

2.3. Synthesis of Co(II), Ni(II) and Cu(II) complexes

A hot ethanolic solution of the hydrated MCl_2 (M = Cu, Co, Ni) (1.0 mmol) (25 ml), was added to hot ethanolic solution of H_2OPPAH (1.0 mmol) in a hot ethanol (25 ml). The reaction mixture was heated under reflux for 4 h. The formed precipitates were filtered off, washed with ethanol followed by diethyl ether and then dried in a desiccator over anhydrous $CaCl_2$.The complexes are stable in air.

2.4. Computational details

We performed cluster calculations using DMOL^3 program (Wu & Ray, 2002) in Materials Studio package (Hehre et al., 1986), which is designed for the realization of large scale density functional theory (DFT) calculations. DFT semi-core pseudopods calculations (dspp) were performed with the double numerica basis sets plus polarization functional (DNP). The DNP basis sets are of comparable quality to 6-31G Gaussian basis sets. Delley et al. showed that the DNP basis sets are more accurate than Gaussian basis sets of the same size.The RPBE functional (Delley 2002) is so far the best exchange-correlation functional (Matveev et al., 1999), based on the generalized gradient approximation (GGA), is employed to take account of the exchange and correlation effects of electrons. The geometric

optimization is performed without any symmetry restriction.

2.5. Biological studies

2.5.1. Antioxidant activity screening assay ABTS method

The antioxidant activity assay(Lissi et al., 1999 and El-Gazzar et al., 2009) employed is a technique depending on measuring the consumption of stable free radicals i.e. evaluate the free radical scavenging activity of the investigated component. The methodology assumes that the consumption of the stable free radical (X') will be determined by reactions as follows:

$$X' + YH \rightarrow XH + Y'$$

The rate and / or the extent of the process measured in terms of the decrease in X' concentration, would be related to the ability of the added compounds to trap free radicals. The decrease in color intensity of the free radical solution due to scavenging of the free radical by the antioxidant material is measured colorimetrically at a specific wavelength. The assay employs the radical cation derived from 2, 2′- Azino-bis (3-ethyl Benzthiazoline-6-sulfonic acid) (ABTS) to assess antioxidant and extracts. The reaction mixture (Negative control) consists of 2 ml of 2,2′-azino-bis-(3-ethyl benzthiazoline-6-sulfonic acid) (ABTS) solution (60 µl) and 3 ml of MnO_2 solution (25 mg/ml), all prepared in phosphate buffer (pH=7). The mixture was shaken, centrifuged and filtered to remove the excess oxide. The absorbance (A control) of the resulting green-blue solution (ABTS+ radical solution) was recorded at λ_{max}=734 nm. The absorbance (A_{sample}) was measured upon the addition of 20 µl of 1 mg/ml solution of the test sample under investigation in spectroscopic grade MeOH/buffer (1:1 v/v) to the ABTS solution. Ascorbic acid 20 µl (2ml) solution was used as standard antioxidant (positive control). Blank sample was run using solvent without ABTS. The decrease in absorbance is expressed as % inhibition. The Inhibition percent of the free radical ABTS was calculated according to the equation:

$$I\% = (A_{blank} - A_{sample}) / (A_{blank}) \times 100$$

Where A_{blank} is the absorbance of the control reaction (containing all reagents except the test compound), and A_{sample} is the absorbance of the test sample.

2.5.2. Antioxidant activity screening assay for erythrocyte hemolysis

The blood was obtained from rats by cardiac puncture and collected in heparinized tubes. Erythrocytes were separated from plasma and the buffy coat was washed three times with 10 volumes of 0.15 M NaCl. During the last wash, the erythrocytes were centrifuged at 2500 rev. /min for 10 min to obtain a constantly packed cell preparation. Erythrocyte hemolysis was mediated by peroxyl radicals in this assay system (Morimoto et al., 1995). A 10% suspension of erythrocytes in phosphate buffered saline pH 7.4 (PBS) was added to the same volume of 200 m MAAPH solution in PBS containing samples to be tested at different concentrations. The reaction mixture was shaken gently while being incubated at 37 °C for 2 h. The reaction mixture was then removed, diluted with eight volumes of PBS and centrifuged at 1500g for 10 min. The absorbance of the supernatant was read at 540 nm. Similarly, the reaction mixture was treated with 8 volumes of distilled water to achieve complete hemolysis, and the absorbance of the supernatant obtained after centrifugation was measured at 540 nm. The data percentage hemolysis was expressed as mean ±standard deviation. L-ascorbic acid was used as a positive control.

2.5.3. Cytotoxic activity

2.5.3.1. Ehrlich cells

Ehrlich cells (Ehrlich ascites Carcinoma, EAC) were derived from ascetic fluid from diseased mouse (the cells were purchased from National Cancer institute, Cairo, Egypt which is acertified institute by National Medical Research Ethics Committee). DNA (Calf Thymus type1), bleomycin sulfate, butylatedhydroxyanisole (BHA), thiobarbituric acid (TBA), ethylenediaminetetraacetic acid (EDTA) and ascorbic acid were obtained from sigma. 2, 20-azo-bis-(2-amidinopropane)

dihydrochlorid (AAPH), 2,2 /-azino-bis-3-ethylbenzthiazoline-6-sulfonic acid (ABTS) were purchased from Wako Co., USA.

2.5.3.2. Antitumor activity using Ehrlich ascites in vitro assay

Different concentrations of the tested compounds were prepared (100, 50 and 25 ml from 1 mg/mL in DMSO (<00.05%, v/v) and RPMI-1640 medium). The ascites fluid from the peritoneal cavity of the diseased mouse (contains Ehrlich cells) was aseptically aspirated. The cells were grown partly floating and partly attached in a suspension culture in RPMI-1640 medium, supplemented with 10% fetal bovine serum. They were maintained at 37 °C in a humidified atmosphere with 5% CO_2 for 2 h. The viability of the cells determined by the microscopical examination using a hemocytometer and using trypan blue stain (stains only the dead cells) (Fadda et al., 2010).

3. Results and Discussion

The data of physical properties and elemental analysis of the complexes are summarized in Table 1.The complexes are insoluble in water or nonpolar organic solvents but soluble in DMF solvent.The values of molar conductivity of all complexes lie in the range (5-17 ohm^{-1} cm^2 mol^{-1}) indicating their non-electrolytic nature (Fadda et al., 2010).Unfortunately, we could not get single crystals from the solid metal complexes.

Table (1): Analytical and physical data of H_2OPPAH and its complexes.

Compound Empirical formula, (F.Wt)	Colour	M.p. (°C)	% Found (Calcd.)				Yield (%)
			M	Cl	C	H	
H_2OPPAH $C_{15}H_{14}N_4O_2$ (282.3)	White	260	-	-	63.79 (63.82)	4.99 (5.00)	85
$[Cu(H_2OPPAH)Cl_2(H_2O)].H_2O$ $CuC_{15}H_{18}N_4O_4Cl_2$ (452.78)	Brown	>300	14.70 (14.03)	14.87 (15.66)	39.26 (39.79)	4.00 (4.01)	80
$[Co(HOPPAH)Cl].4H_2O$ $CoC_{15}H_{21}N_4O_6Cl$ (447.74)	Olive green	>300	12.79 (13.16)	8.00 (7.92)	39.04 (40.24)	5.04 (4.73)	85
$[Ni(HOPPAH)Cl(H_2O)_2].H_2O$ $NiC_{15}H_{19}N_4O_5Cl$ (429.48)	Pale brown	>300	14.34 (13.67)	9.02 (8.25)	41.84 (41.95)	4.87 (4.46)	80

3.1. IR Spectra

The most important infrared bands of H_2OPPAH and its metal complexes are depicted in Table 2. A comparison of the spectrum of the ligand and its complexes revealed that the ligand coordinates in the enol form. IR spectrum of H_2OPPAH (in KBr) **(Structure I)** shows two bands at 1648 and 1600 cm^{-1} assignable to $\nu(C=N)_{azomethine}$ and $\nu(C=C)$ phenyl vibrations, respectively (Sreeja et al., 2004). The broad band at 3294 cm^{-1} is due to $\nu(N^4H)$ and $\nu(N^1H)$ modes. This broadness may be referred to the H-bond formation. In the IR spectra of all complexes, the broad band in the region~3121-3295 cm^{-1} arising from overlap of the stretching vibrations of lattice water molecules with the ν(N-H) of the ligand.The bands at 1717 and 1676 cm^{-1} are assignable to bonded $(C=O)^2$ and free carbonyl $(C=O)^3$ vibrational modes (Abu El-Reash et al., 2014) which oriented

themselves in opposite direction to each other as confirmed by molecular modeling. Thus suggesting the presence of one carbonyl in the keto form while the other carbonyl undergoes enolization forming C-OH. This is confirmed by the appearance of new bands at 3336, 1375 and 1227 cm^{-1} assignable to ν(C-OH), δ(OH) and ν(C-O), suggesting the presence of intramolecular hydrogen bonding. In complexes, the first band disappears suggesting enolization followed by deprotonation while the second band undergoes blue shift as a result of coordination to the metal ion. The medium intensity band at 1176 cm^{-1} is assignable to ν(N-N) which undergoes red shift upon complexation due to the increase in the double bond character of N-N offsetting the loss of electron density via donation to the metal ion and is a further evidence of coordination of the ligand through the azomethine nitrogen atom (Chakraborty et al., 2009). The bands observed at 1551, 989, 618 and 406 cm^{-1} are assigned to ν(C=N)pyridine stretching, pyridine- ring breathing modes, in-plane-bending and out-of plane ring vibration modes, respectively (Rakha 2000).

Table (2) : Principle infrared bands of H_2OPPAH and its metal complexes.

Compound	ν(C=C)	$\nu(C=N)_{Py}$	ν(C=N)	$\nu(C=O)^3$	$\nu(C=O)^2$	$\nu(NH)^4$	$\nu(NH)^1$	$\nu(C-O)^2$	ν(N-N)	$\nu(C=N)^*$	ν(M-O)	ν(M-N)
H_2OPPAH	1600	1551	1648	1676	1717	3294	3294	-	1176	-	-	-
$[Cu(H_2OPPAH)Cl_2(H_2O)].H_2O$	1598	1530	1633	1678	-	3295	-	1240	1196	1633	502	466
$[Co(HOPPAH)Cl].4H_2O$	1600	1537	1625	1683	-	3294	-	1242	1191	1619	512	452
$[Ni(HOPPAH)Cl(H_2O)_2].H_2O$	1598	1568	1646	1675	-	3295	-	1240	1187	1646	522	483

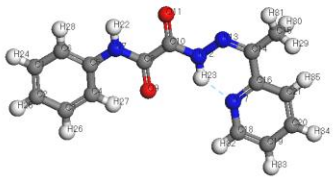

(a)

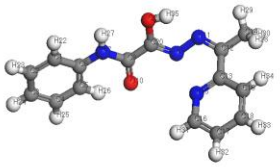

(b)

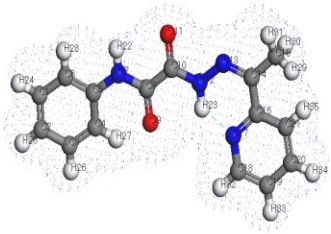

(c)

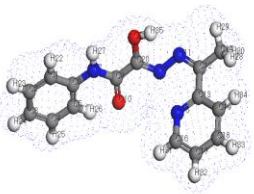

(d)

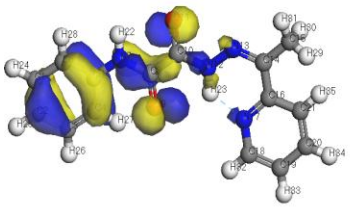

(e)

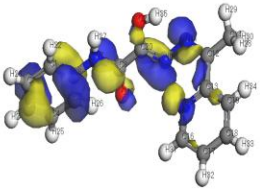

(f)

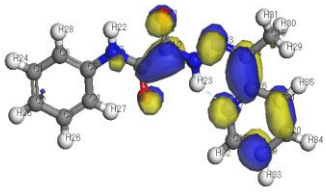

(g)

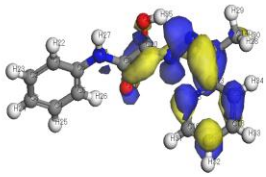

(h)

Structure I

Keto Form

(a)Molecular modeling of H_2OPPAH

(c)Electron density

(e)HOMO and (g) LUMO

Enol Form

(b) Molecular modeling

(d) Electron density

(f) HOMO and (h) LUMO

H_2OPPAH behaves as a mononegative NNO tridentate in $[Co(HOPPAH)Cl].4H_2O$ and $[Ni(HOPPAH)Cl(H_2O)_2].H_2O$ complexes **(Structures II&III)** through $(C=N)_{py}$, $(C=N)_{azomethine}$ and deprotonated $(C-OH)^2$ groups while the other carbonyl group, $(C=O)^3$ remains at the same position without participating in coordination. This behavior is revealed by the disappearance of bands due $\nu(C=O)^2$ and $\nu(N^1H)$ modes with simultaneous appearance of new broad bands at (1619 & 1646 cm^{-1}) and (1242 & 1240) cm^{-1}, respectively attributable to the new ν (C=N-N=C)* and ν(C-O) vibrations. The bands assignable to ν/δ $(C=N)_{py}$ shift either to lower wavenumber by ~ 14 cm^{-1} in case of Co(II) complex or to higher wavenumber by ~17 cm^{-1} in case of Ni(II) complex , indicating coordination of the metal ion to pyridine nitrogen (Rakha 2000). Also, the negative shift of $\nu(C=N)_{azomethine}$ confirming its participation in coordination. On the other hand, in $[Cu(H_2OPPAH)Cl_2(H_2O)].H_2O$ complex **(Structure IV)**, the ligand coordinated as neutral NNO tridentate via $(C=O)^3$, $(C=N)_{py}$ and $(C=N)_{azomethine}$ groups as confirmed by the shift of bands due to the aforementioned groups to lower wavenumber. The presence of

band at 3333cm^{-1} in the spectrum of this complex attributed to ν(C-OH) [2] suggest the rearrangement and enolization of this group without involving in coordination pyridine nitrogen (Abu El-Reash et al., 2014) . This is also revealed by the new bands at 1633, 1319 and 1240 cm^{-1}, respectively assignable to new ν (C=N-N=C)*, δ(OH) and ν(C-O) modes.

The new bands observed in the IR spectra all complexes at 502-537 and 442-489 cm^{-1} are tentatively assigned to the ν(M-O) (Schrader 2007) and ν(M-N) (Atmeh et al., 2008), respectively confirming the suggested mode of chelation. Also, the IR spectra of Ni(II) and Cu(II) complexes exhibit bands at ≈ 3399-3454, 868-850, and at ≈ 567cm^{-1} referred to Δ(H_2O), p_r (H_2O) and P_w (H_2O) vibrations for the coordinated water. The broad band centered at ~ 3500 cm^{-1} in the spectra of all complexes may be due to hydrated water. This notification will be supported by thermal analysis

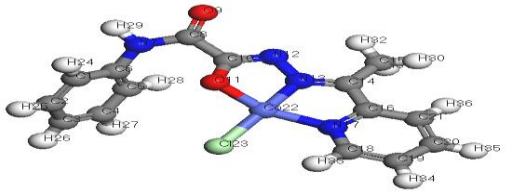

Structure II: Molecular modeling of [Co(HOPPAH)Cl].4H_2O

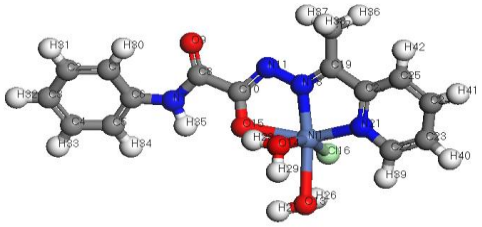

Structure III: Molecular modeling of [Ni(HOPPAH)Cl(H_2O)$_2$].H_2O

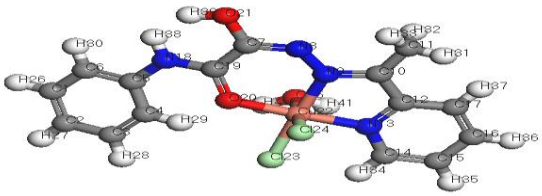

Structure IV: Molecular modeling of [Cu(H_2OPPAH)Cl_2(H_2O)].H_2O

3.2.^{1}H-NMR spectra

The ^{1}H NMR spectrum of the ligand H_2OPPAH in DMSO-d_6 **(Fig. 1a)** as a solvent confirmed the presence of two tautomeric forms of the Schiff base ligand **(Structure I)** in solution under the experimental conditions. In ^{1}H NMR, the appearance of a signal at 15.78 ppm (*i.e.* high value downfield from TMS) assignable to -C^2 -OH proton **(In Structure Ib: C20-OH)**. Signals at 11.16 and 10.97 ppm assignable to the protons of (N^{4}H) and (N^{1}H), respectively of the keto form while the signal at 10.92 ppm assignable to (N^{4}H) of the enol form. All the previous signals disappeared upon adding D_2O **(Fig. 1b)**. The keto: enol ratio could be assessed for about 71%: 29%. The signals of all hydrogen among the aromatic ring and pyridine rings are duplicated (7.23 – 8.90 ppm) equivalent to 18 protons suggesting the existence of keto and enol tautomers. The signals at δ3.38-3.36 ppm may be equivalent to 6 protons of the two CH_3 groups.

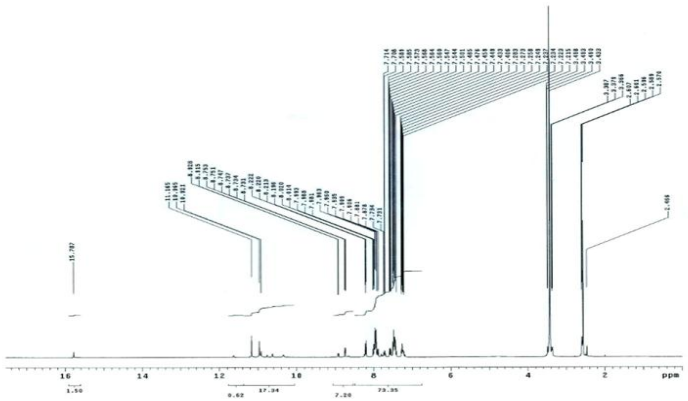

Fig.(1)a: ^{1}H NMR spectrum of H_2OPPAH in d_6-DMSO.

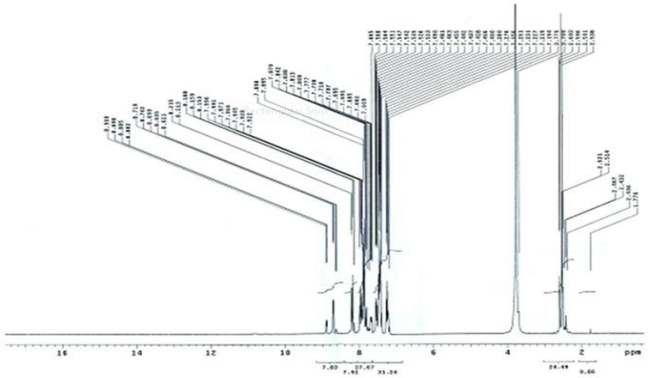

Fig.(1)b: ^{1}H NMR spectrum of H_2OPPAH in D_2O.

3.3. Electronic Spectra and magnetic measurements

Electronic spectra of the ligand and its metal complexes were displayed in dimethylsulfoxide (DMSO) solution or Nujol mull. No difference was observed on using both solvents. The tentative assignments of the significant spectral absorption bands, magnetic moments and ligand field parameters of metal complexes are given in Table 3.The electronic spectrum of H_2OPPAH shows an intense absorption band at 303030 cm^{-1} assignable to $\pi \rightarrow \pi^*$ transition of pyridine and benzene rings. A red shift is observed for this transition in the spectra of complexes as a result of coordination of the nitrogen of the pyridine ring (Rakha et al., 2014). Another intense absorption band is observed at 28735 cm^{-1} attributable to $\pi \rightarrow \pi^*$ of azomethine and carbonyl groups which shift in complexes toward higher frequencies, supporting the coordination of the azomethine nitrogen and carbonyl oxygen atoms with the central metal ion (El-Gammal et al., 2012). The band at 25445 cm^{-1} attributable to $(n\rightarrow\pi^*)_{py}$, transition.The bands in the 21929-19724 cm^{-1} region attributable to $n\rightarrow\pi^*$ transition of the two carbonyl groups. The $Cl\rightarrow M^{2+}$ transition is generally found in the 27173- 28783 cm^{-1} region and would contribute to the higher energy $n\longrightarrow\pi^*$ band.

The electronic spectrum of [Co(HOPPAH)Cl].$4H_2O$ in Nujol exhibits a well-defined bands at 16722 and 19783 cm^{-1}. The second band is assigned to $^{4}A_2(F) \rightarrow {}^{4}T_1(F)(\nu 3)$ transition characteristic for tetrahedral geometry. The band in the region 4500-7500 cm^{-1} cannot be observed due to restriction of our equipment. The dark green color is an additional evidence for this structure. The values of ligand field parameters (Dq, B and β) are 542 cm^{-1}, 593 cm^{-1} and 0.61 which are typical for tetrahedral Co^{2+} complexes (El-Gammal et al., 2014). The value

of β indicates an appreciable degree of covalence of the Co (II) ligand bonds. Also, the magnetic moment value (3.79 B.M.) is consistent with the proposed geometry.

The UV spectrum of $[Ni(HOPPAH)Cl(H_2O)_2].H_2O$ complex displays two bands at 18967 and 27173 cm^{-1} assignable to $^3A_{2g} \rightarrow ^3T_{1g}(F)(\nu_2)$ and $^3A_{2g} \rightarrow ^3T_{1g}(P)(\nu_3)$ transitions (Sathyadevi et al., 2012), respectively, in an octahedral geometry. The calculated values of ligand field parameters lie in the range reported for an octahedral environment around nickel (II) ion. The low magnetic moment value (1.89 BM.) is attributed to strong M-M interaction.

The electronic spectrum of $[Cu(H_2OPPAH)Cl_2(H_2O)].H_2O$ complex exhibits two bands: an asymmetric broad band at 19305 cm^{-1} and a more intense band at 23596 cm^{-1}. The latter band may be assigned to ligand metal charge transfer transition. The first band is assignable to d–d band appears as broad or weak shoulder in the tail of CT bands and is due to $^2B_{1g} \rightarrow ^2E_g$ and $^2B_{1g} \rightarrow ^2A_{1g}$ transitions, respectively, in an octahedral environment. Also, the band at 20933 cm^{-1} is due to Cl→Cu(II) transition (Seena & Kurup, 2008). The low magnetic moment (1.59 B.M.) reveals M-M interaction.

Table (3): Spectral absorption bands, magnetic moments and ligand field parameters of H_2OPPAH metal complexes.

Compound	Band position , cm^{-1}	Assignment	Ligand field parameters			μ_{eff} (B.M.)
			D_q (cm^{-1})	B (cm^{-1})	β	
H_2OPPAH	303030,287356, 254452,219298, 197238	$\pi \longrightarrow \pi^*$ $n \longrightarrow \pi^*$	-	-	-	-
$[Cu(H_2OPPAH)Cl_2(H_2O)].H_2O$	33783,28789, 23596,20933, 19305	$^2B_{1g} \longrightarrow ^2E_g$ $^2B_{1g} \longrightarrow ^2A_{1g}$ LMCT	-	-	-	1.59
$[Ni(HOPPAH)Cl(H_2O)_2].H_2O$	27173,21929, 18967	$^3A_{2g} \longrightarrow ^3T_{1g}(P)$ $^3A_{2g} \longrightarrow ^3T_{1g}(F)$	599	649	0.62	1.89
$[Co(HOPPAH)Cl].4H_2O$	32994,28825, 22524,19783, 16722	$^4A_2(F) \longrightarrow ^4T_1(F)$	542	593	0.61	3.79

3.4. Electron spin resonance

The ESR spectrum of $[Cu(H_2OPPAH)Cl_2(H_2O)].H_2O$ complex (Fig.2) exhibits broad single line, nearly isotropic signal centered at $g_{\|}$= 2.098 and $g_{\perp}$= 2.076, respectively attributable to dipolar broadening and enhanced spin lattice relaxation (Yokoi et al., 1975). This line broadening is probably due to insufficient spin-exchange narrowing toward the coalescence of four copper hyperfine lines to a single line. Note that, the same kind of powder ESR line shapes; have also been observed for many tetrahedral or square planar binuclear Cu (II) complexes with a considerably strong intranuclear spin-exchange interaction (Pal 2002). According to Hathaway (Hathaway & Billing, 1970 and Hathaway 1984), as value of G is greater than 4, the exchange interaction between copper (II) centers in the solid state is negligible, whereas when it is less than 4, a considerable exchange interaction is indicated in

the solid complex. The calculated G value for the present copper complex is 1.29 which is less than 4 suggesting copper–copper exchange interactions which is in accordance with the subnormal magnetic moment ($\mu_{eff.}$ = 1.59 B.M.). The axially symmetric g-tensor parameters with $g_{\parallel} > g_{\perp} > 2.0023$ indicate that the copper site has a $d_{x^2-y^2}$ ground-state characteristic of square planar or octahedral stereochemistry (Kasumo 2001) and reveal an appreciable covalence of the metal ligand bonding .

To quantify the degree of distortion of the Cu(II) complex, the f-factor, $g_{\parallel}/A_{\parallel}$ was calculated which is considered as an empirical index of tetrahedral distortion (Annigeri et al., 2008). Its value ranges between 105 and 135 for square planar complexes, depending on the nature of the coordinated atoms. In the presence of a distorted tetrahedral structure, the values can be much larger. In the present case the value is 128 demonstrating the presence of significant dihedral angle distortion in the xy-plane and indicating a tetrahedral distortion from octahedral geometry and the results are consistent with distorted octahedral geometry around the copper site.

This is in accordance with the weak bond between the axial pyridine nitrogen and the copper (II) ion as determined by molecular modeling.

Molecular orbital coefficients, α^2 (a measure of the covalence of the in-plane σ-bonding between a copper 3d-orbital and the ligand orbitals) and β^2 (covalent in-plane π-bonding), were calculated by using the following equations (Jayasubramanian et al., 1995 and Anthonisamy & Murugesan, 1998):

$$\alpha^2 = (A_{\parallel}/0.036) + (g_{\parallel} - 2.0023) + 3\,(g_{\perp} - 2.0023)/7 + 0.04 \quad \textbf{(1)}$$

$$\beta^2 = (g_{\parallel} - 2.0023)\,E/ - 8\lambda\alpha^2 \quad \textbf{(2)}$$

Where λ=-828 cm^{-1} for the free copper ion and E is the electronic transition energy.

As a measure of the covalence of the in-plane σ-bonding α^2 = 1 indicates complete ionic character, whereas α^2 = 0.5 denotes 100% covalent bonding, with the assumption of negligibly small values of the overlap integral. The β^2 parameter gives an indication of the covalence of the in-plane π-bonding. The smaller the β^2 value, the larger the covalence of the bonding.

The values of α^2 and β^2 for this complex (0.45 & 0.62) indicate that the in-plane σ-bonding and in-plane π-bonding are appreciably covalent and again supports the fact that enolato oxygen binding in the present copper complex incorporates significant covalence in the metal-ligand bonding through delocalized d_{π}—p_{π} in plane π-bonding (Raman et al., 2001). For the octahedral complexes, the lower values of β^2 compared to α^2 indicate that the in-plane π-bonding is more covalent than the in-plane σ-bonding. These data are well consistent with other reported values (John 2003 and Abu El-Reash et al., 2013).

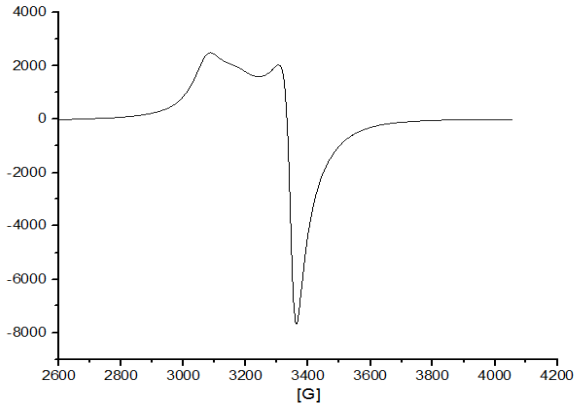

Fig.(2): ESR spectrum of $[Cu(H_2OPPAH)Cl_2(H_2O)].H_2O$ at room temperature.

3.5. Mass spectra

The mass spectrum of H_2OPPAH is given in (Fig.3) as a representative example shows the molecular ion peak at m/z = 282.4 (5.25%) corresponding to ($C_{15}H_{14}N_4O_2$) (Refat 2007). The different fragments of H_2OPPAH give the peaks with various intensities at different m/z values like at 196.4(4.78%)($C_3H_4N_2O$), 106.2(16.84%)(C_6H_6N) and 79.00(22.12%)(CO). The base peak at m/z 76.80 represents C_5H_4N with Rel.Int.:100%.

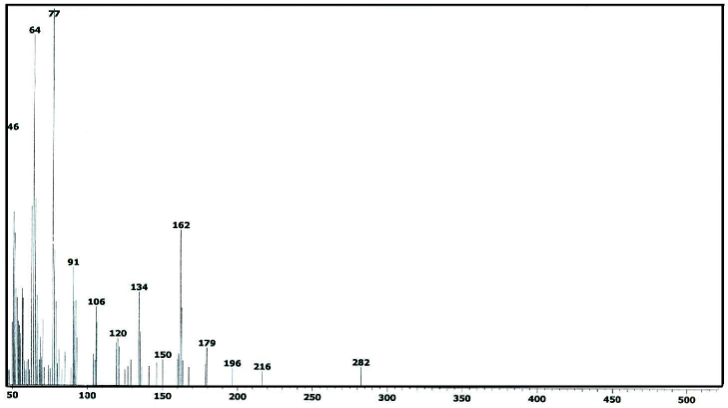

Fig. (3): Mass spectrum of H_2OPPAH.

3.6. Thermogravimetric studies

The stages of decomposition, temperature range, decomposition product as well as the weight loss percentages of the complexes are given in Table 4. (Fig.4) shows the TGA curves of the metal complexes.Thermal data showed that the crystal water molecules are volatilized within the temperature range 43-129°C, while the coordinated water molecules are removed in the temperature range 130-351°C. The TGA of [Ni(HOPPAH)Cl(H_2O)$_2$].H_2O complex was discussed in detail as a representative example. The TG curve of complex displays 4.30 % weight loss (Calcd. 4.19 %) in the temperature range 43 - 129^{o}C which correlated to one water molecule outside the coordination sphere. Thermal degradation of the organic molecule starts above 129°C. In the temperature range 130-351°C, the weight loss (Found: 17.32% ;(Calcd. 16.87 %)) in the TG curve is attributed to the elimination of $2H_2O$+HCl fragments. In 352-594^{o}C, it is almost probably assigned to the elimination of the loosely bound (CH_3CN) moiety with weight loss: 10.00 (Calcd. 9.55 %). In the temperature range 595-707°C, the weight loss (Found: 6.09% ;(Calcd. 6.51 %)) in the TG curve is attributed to the elimination of N_2 fragment, after which aconstant weight was observed while C_5H_4N+ C_6H_5O+NiO+2C become the residual part with 62.29 % (Calcd. 62.88 %) weight loss. It is clear that, the TG thermogrames for the investigated complexes displayed high residual part indicating high stability of the formed chelates

.

Table (4): Decomposition steps with the temperature range and weight loss for H_2OPPAH and its complexes.

Complex	Temp. Range,°C	Removed species	Wt. Loss	
			Found%	Calcd.%
H_2OPPAH	129-494	- C_6H_6+C_5H_6N+H_2O+CO+N_3	88.36	87.22
	494-800	- 3C(Residue)	11.63	12.77
[Ni(HOPPAH)Cl(H_2O)$_2$].H_2O	43-129	- H_2O	4.30	4.19
	130-351	-2H_2O+HCl	17.32	16.87
	352-594	-CH_3CN	10.00	9.55
	595-707	-N_2	6.09	6.51
	707-800	- C_5H_4N+ C_6H_5O+NiO+2C(Residue)	62.29	62.88
[Co(HOPPAH)Cl].4H_2O	26-264	- 4H_2O+ HCl+ CH_3CN	33.70	33.40
	265-466	- C_5H_4N	16.55	17.44
	467-626	-N_2	6.41	6.25
	626-800	- C_6H_5O+CoO+2C(Residue)	43.34	42.91
[Cu(H_2OPPAH)Cl_2(H_2O)].H_2O	74-263	- 2H_2O+2HCl +N_2	30.58	30.24
	264-534	- CH_3CN + C_5H_4N	27.06	26.31
	534-800	- C_6H_5O+CuO+2C(Residue)	42.36	43.45

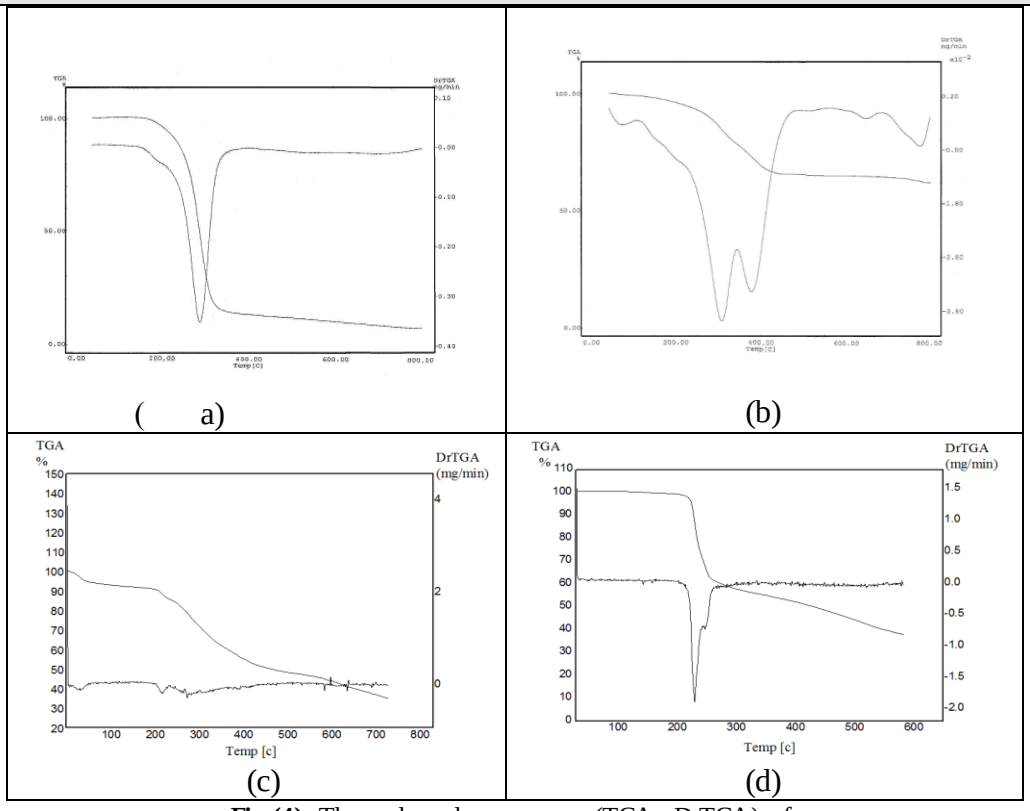

Fig.(4): Thermal analyses curves (TGA , D_rTGA) of:
(a) H_2OPPAH **(b)** [Ni(HOPPAH)Cl(H_2O)$_2$].H_2O
(c) [Co(HOPPAH)Cl].4H_2O **(d)** [Cu(H_2OPPAH)Cl_2(H_2O)].H_2O

3.7. Kinetic data

The kinetic parameters such as activation energy (E_a), pre-exponential factor (A) were determined using Coats-Redfern (Coats & Redfern, 1964) and Horowitz-Metzger (Horowitz & Metzger, 1963) methods. Thermodynamic parameters such as entropy of activation (ΔS*), enthalpy of activation (ΔH*) and free energy of activation (ΔG*) of decomposition steps were calculated by Eyring equation (Broido 1969):

$$\Delta H^* = E_a - RT \quad (3)$$

$$\Delta S^* = R \ln \frac{hA}{k_B T} \quad (4)$$

$$\Delta G^* = \Delta H^* - T\Delta S^* \quad (5)$$

In both methods, the lift side of equations 3 and 4 are plotted against 1/T and θ, respectively as shown in Figs.(5& 6). The data obtained are recorded in Tables 5 &6. A glance at the Tables indicate that the high values of the energy of activation, E of the complexes reveals the high stability of such chelates due to their covalent bond character (Frost & Pearson, 1961).The positive sign of ΔG for the investigated complexes reveals that the free energy of the final residue is higher than that of the initial compound, and all the decomposition steps are non-spontaneous processes. Also, the values of the activation, ΔG increases significantly for the subsequent decomposition stages of a given complex. This is due to increasing the values of TΔS significantly from one step to another which overrides the values of ΔH (Hatakeyama & Quinn, 1994).The negative values of ΔS for the degradation process indicates more ordered activated complex than the reactants or the reaction is slow.

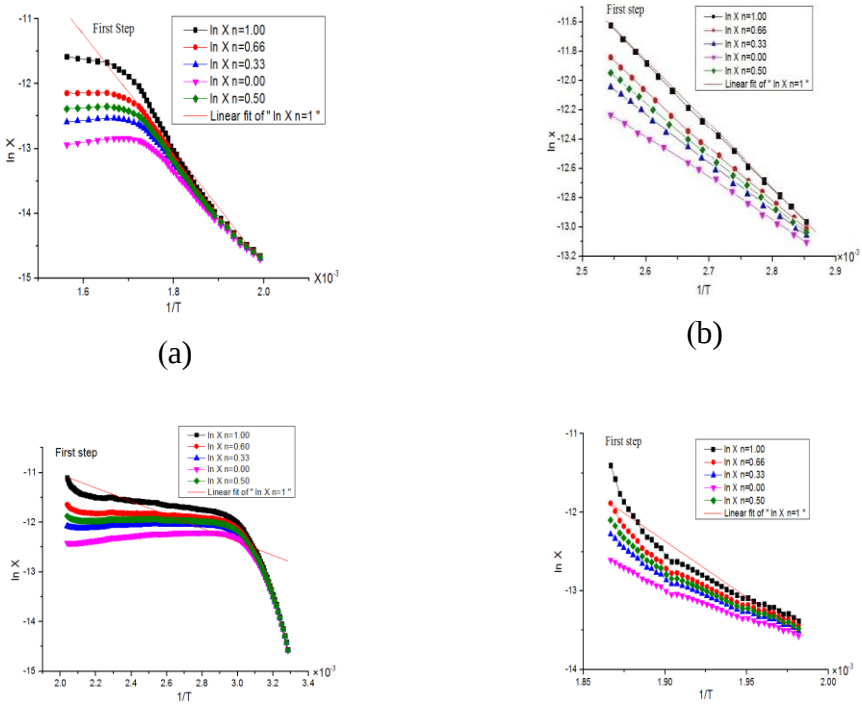

Fig.(5): Coats-Redfern plots of 1st step degradation of:

(a) H_2OPPAH **(b)** $[Ni(HOPPAH)Cl(H_2O)_2].H_2O$
(c) $[Co(HOPPAH)Cl].4H_2O$ **(d)** $[Cu(H_2OPPAH)Cl_2(H_2O)].H_2O$

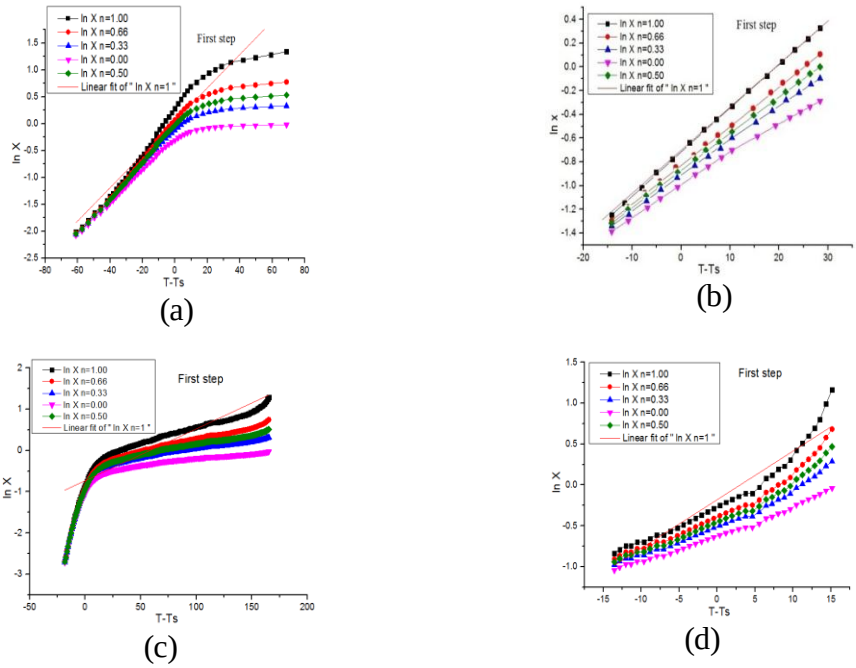

Fig.(6): Horowitz–Metzger plots of 1st step degradation of:

(a) H_2OPPAH **(b)** $[Ni(HOPPAH)Cl(H_2O)_2].H_2O$
(c) $[Co(HOPPAH)Cl].4H_2O$ **(d)** $[Cu(H_2OPPAH)Cl_2(H_2O)].H_2O$

Table (5): Kinetic Parameters evaluated by Coats-Redfern equation for H_2OPPAH and its complexes.

complex	Peak	Mid Temp(K)	Ea KJ/mol	A (S^{-1})	ΔH* KJ/mol	ΔS* KJ/mol.K	ΔG* KJ/mol
H_2OPPAH	1st	570.85	74.17	$4.64x10^4$	69.42	-0.1610	161.32
$[Co(HOPPAH)Cl].4H_2O$	1st	397.56	11.29	$1.40x10^6$	7.98	-0.1297	59.53
	2nd	657.46	47.76	$7.39x10^4$	42.30	-0.1583	146.36
	3rd	820.65	94.13	$2.95x10^3$	87.30	-0.1869	240.69
$[Cu(H_2OPPAH)Cl_2(H_2O)].H_2O$	1st	520.15	118.73	$9.25x10^9$	114.41	-0.0588	144.97
	2nd	648.15	23.21	$1.67x10^6$	17.82	-0.1322	103.53
$[Ni(HOPPAH)Cl(H_2O)_2].H_2O$	1st	364.64	36.01	$2.00x10^3$	32.98	-0.1834	99.86
	2nd	536.11	40.71	$8.21x10^4$	36.25	-0.1557	119.73
	3rd	690.08	86.92	$2.60x10^4$	81.18	-0.1674	196.69
	4th	945.49	15.72	$4.50x10^9$	7.86	-0.0697	73.76

Table (6): Kinetic Parameters evaluated by Horowitz–Metzger equation for H_2OPPAH and its complexes

complex	Peak	Mid Temp(K)	Ea KJ/mol	A (S^{-1})	ΔH* KJ/mol	ΔS* KJ/mol.K	ΔG* KJ/mol
H_2OPPAH	1st	570.85	83.99	$3.94x10^{5}$	79.24	-0.1432	160.98
$[Co(HOPPAH)Cl].4H_2O$	1st	325.28	11.04	$8.95x10^{-2}$	8.34	-0.2657	94.76
	2nd	582.05	46.98	$1.89x10^{2}$	42.14	-0.2069	162.57
	3rd	773.10	94.56	$3.28x10^{3}$	88.14	-0.1855	231.56
$[Cu(H_2OPPAH)Cl_2(H_2O)].H_2O$	1st	520.55	133.84	$3.34x10^{11}$	129.51	-0.0289	144.57
	2nd	583.80	26.35	$6.75x10^{-1}$	21.50	-0.2538	169.65
$[Ni(HOPPAH)Cl(H_2O)_2].H_2O$	1st	364.64	40.86	$3.21x10^{3}$	37.83	-0.1795	103.27
	2nd	536.11	51.40	$2.35x10^{2}$	46.94	-0.2044	156.52
	3rd	690.08	80.25	$7.78x10^{3}$	74.52	-0.1774	196.93
	4th	945.49	0.00	$8.56x10^{-16}$	-7.86	-0.5430	505.50

3.8. Chemical reactivity

3.8.1. Global reactivity descriptors

The determination of energies of the HOMO (π donor) and LUMO (π acceptor) are important parameters in quantum chemical calculations (Table7). The E_{HOMO} and E_{LUMO} and their neighboring orbitals are all negative, which indicate that the prepared molecules are stable (Rakha et al., 2014).

DFT method concept the chemical reactivity and site selectivity of the molecular systems. The energies of frontier molecular orbitals (E_{HOMO}, E_{LUMO}), energy band gap which explains the eventual charge transfer interaction within the molecule, electronegativity (χ), chemical potential (μ), global hardness (η), global softness (S) and global electrophilicity index (ω) are calculated using the standard equations (Govindarajan et al., 2012) and are listed in Table 7.

Table (7): Calculated E_{HOMO}, E_{LUMO}, energy band gap ($E_H - E_L$), chemical potential (μ), electronegativity (χ), global hardness (η), global softness (S), global electrophilicity index (ω) and softness (σ) for H_2OPPAH and its complexes.

Compound	E_H / eV	E_L / eV	(E_H-E_L) /eV	χ / eV	μ / eV	η / eV	S / eV^{-1}	ω / eV	σ / eV^{-1}
H_2OPPAH	-5.051	-2.499	-2.552	3.775	-3.775	1.276	0.638	-11.8339	0.783699
$[Co(HOPPAH)Cl].4H_2O$	-3.482	-3.09	-0.392	3.286	-3.286	0.196	0.098	-67.0612	5.102041
$[Cu(H_2OPPAH)Cl_2(H_2O)].H_2O$	-5.249	-4.428	-0.821	4.8385	-4.8385	0.4105	0.20525	-47.1474	2.436054
$[Ni(HOPPAH)Cl(H_2O)_2].H_2O$	-4.997	-3.542	-1.455	4.2695	-4.2695	0.7275	0.36375	-23.4749	1.37457

3.8.2. Local reactivity descriptors

The Fukui function indicates the propensity of the electronic density to deform at a given position upon accepting or denoting electrons and is defined as (Parthasarathi et al., 2003):

$$f(\mathrm{r}) = \frac{\delta p(r)}{\delta N} r$$

Where $p(r)$ is the electronic density, N is the number of electrons and r is the external potential exerted by the nucleus.

The results for H_2OPPAH in keto form predict the highest f_k^+ value for N(13) indicates the most favored site for nucleophilic attack. From the values reported in Tables (1S - 4S) (Supplementary Materials), the reactivity order for the nucleophilic case as N(13)>>C(10)>O(11) and C(14). The calculated f_k^- value predicts that the possible sites for electrophilic attack is O(9)>O(11)>C(4)>C(1) site and the radical attack was predicted as O(11) and N(13) site. In [Co(HOPPAH)Cl].4H_2O complex Co(22) has the highest f_k^- value. The reactivity order for the nucleophile f_k^+ is Cl(23)>>C(10)>C(1)>O(11). The calculated f_k^- value predicts that the possible sites for electrophilic attack is Co(22)>C(5)>Cl(23)>N(12) site and the radical attack was predicted at O(11)>Co(22)>C(14)>N(12) site. In [Ni(HOPPAH)Cl(H_2O)$_2$].H_2O complex, the reactivity order for the nucleophilic case is Ni(12)>>Cl(16)>N(11) and C(19) site, while the electrophilic attack is Cl(16)>>O(15)>>O(14) and N(11) site and radical attack is Ni(12) and Cl(16)>N(11)>C(19) site. On comparison of the three kinds of attacks in [Cu(H_2OPPAH)Cl$_2$(H_2O)].H_2O, it is possible to observe that the nucleophilic attack has a greater reactivity compared with the electrophilic and radical attack. The maximum values of the electrophilic reactivity descriptors at Cl(23)>Cu(22)>Cl(24)>O(21) indicate that this site is more prone to electrophilic attack. The observation of the reactive sites by S_k^+ for H_2OPPAH and its complexes are found almost identical to f_k^+.

3.8.3. Molecular modeling

The molecular structure along with atom numbering of H_2OPPAH and its metal complexes are shown. Analysis of the data calculated for the bond lengths and angles for the bond **(Tables S5-S12) (Supplementary Materials)**, one can conclude the following remarks:

1. C(16)-N(17)$_{pyridine}$ and N(13)-C(14)$_{azomethine}$ bond lengths become slightly longer in all complexes as the coordination takes place via N atoms of -C=N-C=N- group that is formed on deprotonation of OH group in complexes (El-Gammal 2010).
2. The C(8)-O(9) and C(10)-O(11) bond distances in all complexes becomes longer due to the formation of the M-O bond which makes the C-O bond weaker .
3. The N(12)-N(13) bond distance is shorten due to forming a double bond character .
4. The complexes can be arranged according to M-N$_{azomethine,}$ bond lengths as follows: Co(22)-N(13) < Ni(12)-N(18) >Cu(22)-N(9); according to M-N$_{pyridine}$: Co(22)-N(17)< Ni(12)-N(21) >Cu(22)-N(13) and M-O; Co(22)–O(11) < Ni(12)-O(15) > Cu(22)-O(20) , respectively reflecting the great strength of the Co-N and Co-O bonds.

3.9. Antioxidant activity

3.9.1. Antioxidant activity using ABTS inhibition and erythrocyte hemolysis

All compounds were tested for antioxidant activity using ABTS assay and rate erythrocyte hemolysis (Table 8). An inspection of the data in the table indicates that H_2OPPAH exhibits the potent anti-oxidative activity. On the other hand, Cu(II) and Co(II) complexes showed moderate activity while Ni(II) complex exhibited weak antioxidant activity. With respect to erythrocyte hemolysis, the compounds can be arranged in the sequence: H_2OPPAH › Ni(II) complex › Co(II) complex. Cu (II) exhibited no activity.

Table (8): Antioxidant Erythrocyte hemolysis assay for H_2OPPAH and its metal complexes.

Compound	ABTS Inhibition (%)	Erythrocyte hemolysis (%)
L-ascorbic acid	88.88	8.99
H_2OPPAH	47.40	7.38
$[Cu(H_2OPPAH)Cl_2(H_2O)].H_2O$	44.07	67.73
$[Co(HOPPAH)Cl].4H_2O$	40.37	2.58
$[Ni(HOPPAH)Cl(H_2O)_2].H_2O$	31.29	5.78

3.9.2. Antitumor activity using in vitro Ehrlich ascites assay

The compounds were screened for their antitumor activity and the data are recorded in Tables(9&10) and represented graphically in Figs.(7a&7b). An insight to the data obtained reveals that H_2OPPAH had the highest cytotoxic activity (59.43%) followed by Co (II) and Cu (II) complexes while Ni(II) complex exhibited no cytotoxic activity. This reveals the fact that the observed lower IC_{50} values in antioxidant assays did demonstrate that the ligand as well as its metal complexes have the potential as drugs to eliminate the radicals.

Table (9): Ehrlich scavenging spectrophotometric assay of various concentrations of H_2OPPAH and its complexes.

Compound / Conc.	Ehrlich inhibition (%)		
	25 ppm	50 ppm	100 ppm
5-Florouracil	30.0	54.6	98.7
H_2OPPAH	22.1	43.3	82.0
$[Cu(H_2OPPAH)Cl_2(H_2O)].H_2O$	17.1	39.2	74.2
$[Co(HOPPAH)Cl].4H_2O$	19.9	41.3	80.5
$[Ni(HOPPAH)Cl(H_2O)_2].H_2O$	19.2	35.4	67.3

Table (10): Ehrlich scavenging capacities (IC_{50}) of H2OPPAH and its metal complexes.

Compound	IC_{50}(µg/ml)
5-Florouracil	46.15
H_2OPPAH	59.43
$[Cu(H_2OPPAH)Cl_2(H_2O)].H_2O$	67.02
$[Co(HOPPAH)Cl].4H_2O$	61.81
$[Ni(HOPPAH)Cl(H_2O)_2].H_2O$	73.04

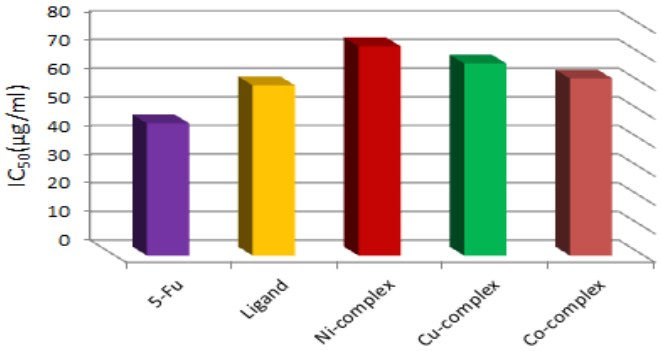

Fig.(7)a: Ehrlich scavenging capacities (IC_{50}) of H_2OPPAH and its metal complexes.

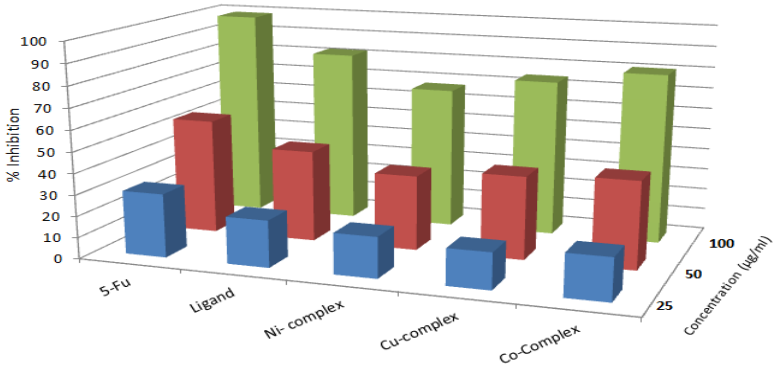

Fig.(7)b: Ehrlich scavenging spectrophotometric assay of various concentrations of H_2OPPAH and its metal complexes.

3.9.3. Structure activity relationship (SAR) studies

The antioxidant, erythrocyte hemolysis and antitumor activities of the investigated compounds is due to the presence of:

i. Two C=O, one $(C=N)_{azomethine}$, two NH and one $(C=N)_{pyridine}$ groups free in the hydrazone, H_2OPPAH moitey. So, it showed the potent antioxidant activity (Abdel-Wahab et al., 2011).
ii. In Co (II) complex, there are still three donor sites free i.e.one C=O, one $(C=N)_{azomethine}$ and one NH groups while in Cu(II) complex only two groups (i.e. NH and $(C=N)_{azomethine}$ that can donate an electron or hydrogen radical thus be converted into a stable diamagnetic molecule.
iii. In case of the Ni (II) complex, although most of the donor sites are free it exhibited weak or no activity.

Conclusion

(Z)-2-oxo-2-(phenylamino)-N'-(1-(pyridin-2-yl)ethylidene)acetohydrazide(H_2OPPAH) and its mononuclear complexes with Co(II), Ni(II) and Cu(II) chlorides were prepared and characterized by conventional techniques. A tetrahedral geometry was proposed for Co (II) complex and an octahedral for Cu (II) and Ni (II) complexes, respectively. The ligand and its complexes were screened for antioxidant activity (using $ABTS^+$), erythrocyte hemolysis and in vitro Ehrlich ascites assay. The relation between the structure of the studied compounds and their activity was discussed. All the data obtained revealed the high activity of ligand and variable activities for other complexes.

References

Abdel-Wahab. B. F, Awad. G. E. A and Badria. F. A ; Eur. J. Med. Chem. 46 **(2011)**1505-1511.

Abu El-Reash. G.M, El-Gammal. O.A, Ghazy. S.E , Radwan. A.H, Spectrochim. Acta A, 104 **(2013)** 26–34.

Abu El-Reash.G.M , El-Gammal. O.A , Radwan. A.H , Spectrochim .Acta Part A,121**(2014)**259-267.

Annigeri. S.M, Sathisha. M.P, Revankar .V.K ; J.Coord.Chem., 61(24) **(2008)** 4011- 4024.

Anthonisamy. V.S.X and Murugesan. R , Chem. Phys. Lett., **(1998)** 287- 353.

Atmeh. M, Russell. N.R, Keyes. T.E, Polyhedron 27 **(2008)** 1690.

Basu. C, Chowdhury. S, Banerjee. R , Evans. H.S, Mukherjee. S, Polyhedron 26**(2007)** 3617.

Bezerra-Netto. H.J.C, Lacerda. D.I, Miranda. A.L.P, Alves. H.M, Barreiro. E.J, Fraga.C.A.M,

Bioorg. Med. Chem. 4 **(2006)** 7924.

Broido. A, J. Polym. Sci., A-2 **(1969)**1761-1773.

Buss. J.L , Neuzil. J , Ponka. P, Biochem. Soc. Trans. 30**(2002)** 755.

Buss. J.L, Neuzil. J, Ponka. P, Biochem. Soc. Trans. 30 **(2002)** 755.

Cescon. L.A, Day. A.R , J. Org. Chem., 27**(1962)** 581-586.

Chakraborty. J, Thakurta. S, Pilet. G, Luneau. D, Mitra. S; Polyhedron 28 **(2009)** 819-825.

Coats. A.W and Redfern. J. P, Nature, 201 **(1964)** 68-69.

Delley. B, Phys. Rev. B 65 **(2002)** 085403.

El-Gammal. O.A , Abu El-Reash. G.M , Ahmed. S.F., J. Mol. Struct.,1007 **(2012)**1-10.

El-Gammal. O.A , Mostafa. M , Spectrochim. Acta Part A 83, **(2014)** 17-27.

El-Gammal. O.A, Abu El-Reash. G.M, Ghazy. S.E, Radwan. A.H, J. Mol.Stru.,1020**(2012)** 6-15.

El-Gammal. O.A, Spectrochim. Acta., A75**(2010)**533-542.

El-Gazzar. A.B.A, Youssef. M.M, Youssef. A.M.S, Abu-Hashem. A.A, Badria. F.A, Eur. J. Med. Chem. 44, **(2009)** 609-624.

Fadda. A.A, Badria. F.A, El-Attar. K.M, Med. Chem. Res. 19 **(2010)** 413-430.

Frost. A.A, Pearson. R .G,"Kinetics and Mechanism", John Wiley, NewYork **1961**.

Getautis .V, Daskeviciene. M , Malinauskas. T, Jankauskas. V, Sidaravicius. J , Thin Solid Films 516 **(2008)** 8979.

Govindarajan. M , Periandy. S , Carthigayen. K , Spectrochim. Acta A 97 **(2012)** 411-422.

Hatakeyama. T, X. F., "Thermal Analysis Fundamentals and Applications to Polymer Science", second ed., John Wiley and Sons, Chichester, **1994**.

Hathaway. B. J, Billing. D.E, Coord. Chem. Rev., 5 **(1970)** 143; Hathaway. B. J, Struct. Bonding (Berlin), 57 **(1984)** 55.

Hehre.W.J, Radom. L, Schleyer. P.V.R, Pople. J.A, "Ab Initio Molecular Orbital Theory", John Wiley, New York, **1986**.

Horowitz. H. H, Metzger. G, Anal. Chem., 25 **(1963)**1464-1468.

Jayasubramanian . K, Samath. S.A, Thambidurai. S, Murugesan. R and Ramalingam . S.K, Trans. Met. Chem., **(1995)** 20-76.

John. R .P, Spectrochim. Acta, 59(A) **(2003)**1349.

Kasumo. V.T, Spectrochim. Acta, 57(A) **(2001)**1649.

Lissi. E.A, Modak. B, Torres. R, Escobar. J and Urzua. A, Free Radical Res. 30,**(1999)** 471-477.

Matveev. A, Staufer. M, Mayer. M, Rösch. N, International journal of quantum chemistry 75 **(1999)** 863-873.

Modeling and Simulation Solutions for Chemicals and Materials Research. Materials Studio, 6 ed., Accelrys software Inc., San Diego, USA, **2011**.

Morimoto.Y, Tanaka. K, Iwakiri.Y, Tokuhiro. S, Fukushima. S, Takeuchi. Y, Bio. Pharm. Bull. 18 **(1995)** 1417-1422.

Pal.S, Proc. Indian Acad. Sci. (Chem. Sci.), 114 **(2002)** 417-430.

Parthasarathi. R , Padmanabhan. J, Sarkar. U, Maiti. B, Subramanian. V, Chattaraj. P.K, Internet Electronic Journal of Molecular Design 2 **(2003)**798-813.

Pérez-Rebolledo. A, Piro. O.E, Castellano. E.E, Teixeira. L.R, Batista. A.A, Beraldo. H , J. Mol.

Pinto. J.J, Moreno. C, Garca-Vargas. M, Talanta 64 **(2004)** 562.

Pouralimardan. O, Chamayou. A.C, Janiak. C, Hosseini-Monfared. H , Inorg.Chim. Acta 360 **(2007)** 1599.

Rakha. T, Synthesis and Reactivity in Inorganic and Matel-Organic Chemistry 30 **(2000)** 205-224.

Rakha.T.H, El-Gammal.O.A, Metwally.H.M , Abu El-Reash. G.M ; J.Mol.Struct.1062 **(2014)** 96-109.

Raman. N, Raja. Y.P and Kulandaisamy. A, Proc. Indian Acad. Sci., (3) **(2001)**113-183.

Refat. M.S., J.Mol.Struct.842 **(2007)**24-37.

Sathyadevi. P, Krishnamoorthy. P, Jayanthi. E , Butorac. R .R, Cowley. A.H, N. 9666 Dharmaraj, Inorg.ChimActa; 384 **(2012)** 83–96.

Schrader. B, "Vibrational Spectroscopy of Different Classes and States of Compounds", Weinheim, Germany, **2007**.

Seena. E.B and Kurup. M.R.P, Polyhedron 26 **(2008)** 829.

Spek. A.L, PLATON, A Multipurpose Crystallographic Tool, Utrecht University,Utrecht, The Netherlands, **1998**.

Sreeja. P.B, Kurup. M.R.P, Kishore. A, Jasmin. C ; Polyhedron 23 **(2004)** 575-581.

Struct. 794 **(2006)** 18.

Terra. L.H.S.A, Guekezian. M , Gaubeur. I , Matos. J.R , SurezIha. M.E.V, Polyhedron 21**(2002)** 2375.

Vicini. P, Incerti. M , Doytchinova. I.A, La Colla. P, Busonera. B, Loddo. R ., Eur. J.Med. Chem. 41 **(2006)** 624.

Whitnall. M , Richardson. D.R , Semin. Pediatr. Neurol. 13 (3) **(2006)** 186.
Wu. X, Ray.A.K, Phys. Rev. B, 65 **(2002)** 85403-85409.
Yokoi. H, Chikira. M, J. Am. Chem. Soc., 97 **(1975)** 3975.

دراسات تركيبية وتحليلية وبيولوجية لبعض المتراكبات الفلزية للهيدرازونات الجديدة.

د/ علا أحمد السيد الجمال .أ.د/ جابر محمد ابراهيم ابوالريش .منى مفرح حسن سرحان
قسم الكيمياء، كلية العلوم، جامعة المنصورة،مصر.

استهدف البحث تحضير وتوصيف متراكبات جديدة باستخدام التحليل العنصرى والقياسات الحرارية والطيفية متمثلة فى طيف الاشعة تحت الحمراء وطيف الاشعة فوق البنفسجية والرنين النووى المغناطيسى والرنين الالكترونى المغزلى والقياسات المغناطيسية وذلك لمتراكبات من

(Z)-2-oxo-2-(phenylamino)-N'-(1-(pyridin-2-yl) ethylidene)acetohydrazide(H_2OPPAH),
(Z)-2-oxo-2-(phenylamino)-N'-(1-(pyridin-4-yl) ethylidene)acetohydrazide(H_2OPPH)

مع أيونات الكروم والمنجنيز والحديد والكوبلت والنيكل والنحاس والكادميوم والزنك والزئبق واليورانيوم السداسي وعمل دراسة تفصيلية للسلوك الطيفى و الحرارى لهذه المتراكبات. كما أجريت بعض الدراسات النظرية الأخرى باستخدام DFT method . كذلك دراسة النشاط البيولوجى. اقترحت بعض الاشكال الفراغية للمتراكبات المفصولة و ذلك من خلال القياسات المغناطيسية والطيفية. وقد تم التوصل الى الأشكال التالية: هرمى رباعى الاوجه لمتراكبات

[Co(HOPPAH)Cl]. $4H_2O$, [Mn_2(H_2OPPAH)Cl_4]. $2H_2O$,

وثمانى الاوجه لمتراكبات:

[UO_2(HOPPAH)(OAc)].H_2O, [Cr_2(H_2OPPAH)Cl_6(H_2O)$_2$] ,
[Mn(H_2OPPH)Cl_2(H_2O)$_2$].H_2O, [Zn(OPPH)(H_2O)$_4$],

الدراسات الحرارية والمعاملات الحركية تم التعرف عليها من خلال طريقتى

coats-Redfern and Horowitz-(Metzger methods)

تم تأكيد الشكل الفراغى لمتراكبات النحاس و كذلك تحليل درجة التساهمية للرابطة بين المرتبط والايون وتم تاكيد الشكل ثمانى الاوجه باستخدام طيف الرنين المغزلى الالكترونى. تضمن الجزء الأخير دراسة التأثير البيولوجى للمركبات التى تم تحضيرها كمضادات للاكسدة ومضادات للسرطان وكذلك تاثيرها على تحلل كرات الدم الحمراء.